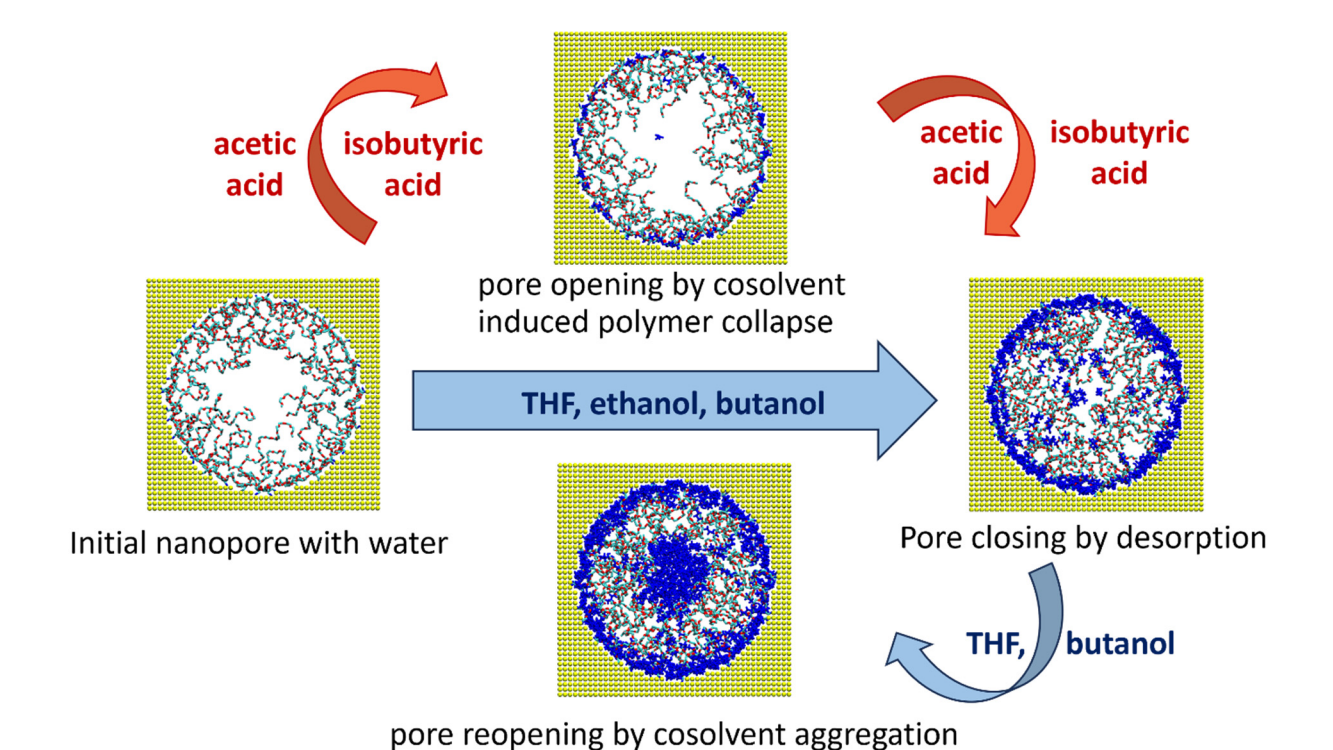
# Cosolvent Induced Gating and Structural Changes in PEO-Grafted Gold Nanopores

Guang Chen† and Elena E. Dormidontova\*,†,‡

†Polymer Program, Institute of Materials Science, University of Connecticut, Storrs, US, 06269 ‡Department of Physics, University of Connecticut, Storrs, US, 06269

E-mail: elena@uconn.edu

## **TOC Graphic** (for Table of Contents use only)



#### **Abstract**

Polymer-grafted nanopores allow control of pore permittivity, which can be exploited in many nanotechnological applications. Using atomistic molecular dynamics simulations, we investigate the effect of cosolvents on the structural properties and gating capability of polyethylene oxide (PEO) grafted gold nanopores filled with cosolvent- aqueous solution. We found that all cosolvents, tetrahydrofuran (THF), ethanol, butanol, acetic acid (ATA) and isobutyric acid (IBA) adsorb onto the nanopore surface releasing water and leading to PEO desorption and expansion into the pore center. This can result in nanopore closure, which occurs at different concentrations depending on cosolvent: ~30-35 volume % for THF and butanol, which are predominantly excluded from the PEO layer and ~50 volume % for ethanol, isobutyric or acetic acids, which interact with PEO chains via hydrogen bonding. We show that further addition of THF or butanol can lead to nanopore reopening due to cosolvent aggregation at the nanopore center compressing the PEO layer. A different mechanism for nanopore opening is found for low concentrations (5% by volume) of acetic and isobutyric acid, which can form hydrogen bonds with PEO and alter its hydration that results in a more compact chain conformation. Lateral water diffusion within the nanopore is shown to be mostly related to the open pore size, while cosolvent diffusion is found to depend also on hydrogen bonding with PEO and cosolvent hydrophobicity.

#### INTRODUCTION

There is a growing interest in controlling the properties of polymer-grafted nanopores for applications in material transport and separation with nano- or micrometer precision<sup>1</sup>, including separation membranes, and selective nanofluidic devices.<sup>2-4</sup> Various triggers that can induce a morphological change in grafted polymers have been investigated to achieve a precise control of nanopore size including pH and voltage for polyelectrolyte brushes<sup>5-8</sup>, light<sup>5</sup> and temperature for thermo-responsive polymer<sup>2,9,10</sup>. Cosolvents can also be used as a trigger to change the polymer conformation, e.g., the coil-globule transition, as has been discussed in detail for solutions<sup>11-14</sup> and to a lesser extent for grafted planar brushes.<sup>15-18</sup> Experimental and theoretical/simulation investigations of cosolvent effects on the conformation of polymers grafted inside the nanopore have so far been rather limited 19-23 and typically have considered just one cosolvent-polymer pair. It would be of great fundamental interest and practical importance to achieve a molecularly detailed understanding of nanopore size control by different cosolvents by comparing the competing interactions (e.g., hydrogen bonding) between polymer, cosolvent, pore surface, and majority solvent (e.g., water), and the associated structural change of the polymer as well as the solvent dynamics, which affects transport properties. To obtain such details atomistic level resolution is required as can be achieved using atomistic molecular dynamics (MD) simulations. This manuscript fulfills this mission by comparing the effects of five cosolvents on the conformational and hydration properties of polyethylene oxide (PEO) grafted inside a gold nanopore and evaluating their gating capability as a function of cosolvent content in aqueous media.

The effect of cosolvent on the properties of a planar grafted polymer brush has been investigated theoretically, 15,24,25 using classical density functional theory (dft), 26 coarsegrained (CG),<sup>17</sup> and atomistic MD simulations<sup>16</sup> by one of us. Analytically it has been predicted that the polymer brush height depends on the effective chi-parameter that describes the interactions of the polymer with both solvents and exhibits a nonlinear dependence on cosolvent concentration. 15,24,25 Non-monotonic changes in the thickness of a polymer layer with cosolvent addition has been also observed in CG simulations.<sup>17</sup> The effect of cosolvent size was analyzed by dft calculations which indicated that a larger cosolvent molecule more effectively screens the excluded volume interactions of the polymer which results in a decreased brush height compared to smaller cosolvents.<sup>26</sup> Using experiments and analytical modeling Yong et. al. found that increased hydrophobicity of different cosolvents (alcohols) enhances a poly(N-isopropylacrylamide) (PNIPAAM) brush collapse. 18 Dahal et. al. studied by atomistic MD simulations PEO planar brushes grafted to a gold surface and found that addition of 80 vol% of tetrahydrofuran (THF) leads to cosolvent adsorption onto the gold surface and THF exclusion from the PEO brush.<sup>16</sup> These planar polymer brush studies demonstrate that cosolvents can be used as an effective trigger by changing the polymer conformation and brush height, even though the effect can be rather complex. Confinement into a nanopore can make the balance of solvation/adsorption effects even more complicated.

Despite the obvious potential of a cosolvent to control grafted polymer conformations, there are only a few studies on the role of cosolvent as a trigger for polymer grafted nanopore gating. It has been shown analytically and experimentally  $^{19}$  that addition of a small amount (5~15% by volume) of ethanol to PNIPAAM grafted nanopores can lead to gated control of

a nanopore due to the coil-globule transition of PNIPAMM brush analogous to that observed for planar PNIPAM brushes in earlier expeirments.<sup>20</sup> To investigate gated control Lim and Deng<sup>27</sup> grafted a gold nanoring with poly(ethylene glycol) (PEG) and studied the PEG collapse by adding 2-propanol as a cosolvent to open the pore. It has also been experimentally demonstrated that polyamide membranes can gain a 4-fold flux increase after 2 wt.% acetone addition (with hexane as the majority solvent), because of the increased pore size (*i.e.*, diminished polymer layer thickness).<sup>21,22</sup> Using CGMD simulations, Li et. al.<sup>23</sup> studied the effects of co-nonsolvent addition (CG beads) on the transport of nanoparticles through a polymer grafted nanopore and obtained the relationships between an effective pore size and monomer-co-nonsolvent interaction strength, that determine the degree of polymer collapse. Using self-consistent field theory and Langevin dynamics simulations Coalson et. al.<sup>28</sup> investigated the role of attractive nanoparticles on a strongly stretched polymer brush and determined that nanoparticles can infiltrate and relax the brush thereby opening the nanopore. While experimentally analyzing ion conductance in PEO-grafted nanopore Ma et. al. found that presence of urea changes the ion flow, which can be attributed to the change in PEO conformation near the nanopore surface, as was indicated by atomistic molecular dynamic simulations.<sup>29</sup> These findings indicate that cosolvent-polymer interactions play an important role and furthermore for amphiphilic polymers such as PNIPAAM, the cosolvent may also change its solubility in water via a change in hydrogen bonding. To gain such details an atomistic level of resolution is required, while so far atomistic MD simulations of cosolvent effects on grafted polymer nanopore gating have been missing. Furthermore, it would be desirable to compare the influence of several cosolvents on the nanopore gating to gain perspective on the effect of the relative hydrophobicity and

propensity for hydrogen bond formation. These are some of the goals of the present manuscript.

PEO has been actively used for nanomaterial modification including grafting within nanopores<sup>27,30</sup> due to its strong water solubility, biocompatibility<sup>31</sup> and protein adsorption inhibition<sup>32,33</sup> as required for biomedical applications. We have previously investigated different regimes of a concave PEO brush grafted within a gold nanopore.<sup>34</sup> For the present study we have chosen a weak PEO brush (overlapping mushrooms) hydrated by water as is achieved at an intermediate grafting density of polymer and a nanopore diameter of 8nm as a reference system to study the gating capability of different cosolvents. Using atomistic molecular dynamics simulations, we investigated the effect of five cosolvents: tetrahydrofuran (THF), ethanol, butanol, acetic acid (ATA) and isobutyric acid (IBA). These cosolvents were chosen to investigate their role in competitive hydrogen bonding with PEO and water, their relative hydrophobicity and ultimately their impact on nanopore gating. THF is a common solvent which is a proton-acceptor like PEO and competes with PEO for hydrogen bonding with water. In our earlier studies we observed the exclusion of THF from a planar PEO brush exposed to a high concentration of THF (80 vol%).<sup>16</sup> Here we will systematically vary the concentration of THF and investigate the effect of THF addition on the properties of PEO brush grafted to a concave surface. Ethanol and butanol are proton donors of different hydrophobicity that are capable of forming hydrogen bonds with PEO, water and themselves. It will be informative to compare the effects of these cosolvents on the PEO layer properties and investigate the similarities and differences in cosolvent distribution within the nanopore as a function of cosolvent concentration. Acetic and isobutyric acids (ATA and IBA respectively) also possess different hydrophilicities and are

capable of hydrogen bond formation with PEO, water and themselves via the carboxylic group. Our previous observations show that IBA addition to PEO aqueous solutions<sup>35,36</sup> resulted in a nonmonotonic change of PEO conformation due to competitive hydrogen bonding and it is interesting to investigate the effects of ATA and IBA on the behavior of PEO grafted within the nanopore. Furthermore, comparing five cosolvents over a broad range of concentrations allows us to provide a molecular picture with atomistic resolution of the local cosolvent/water/PEO distribution within the nanopore, analyze the PEO chain conformation and hydration, and study cosolvent and water dynamics. These are essential static and dynamic details for both a fundamental understanding of grafted polymer behavior under confinement in mixed solvents and providing guidance in the design of nanomaterials with cosolvent controlled polymer-grafted nanopores.

#### **SIMULATION DETAILS**

Atomistic molecular dynamics simulations of PEO-grafted gold nanopores with different cosolvents were performed using the GPU-accelerated Gromacs<sup>37</sup> 2020.4 on the Extreme Science and Engineering Discovery Environment (XSEDE)<sup>38</sup> and the Advanced Cyberinfrastructure Coordination Ecosystem: Services & Support (ACCESS). The gold nanopore was constructed using a fcc lattice with a 4.08 Å lattice constant. The force field parameter of gold atoms was adopted from the literature.<sup>39</sup> Methyl-terminated PEO chains of 20 repeat units (-S-[CH<sub>2</sub>-CH<sub>2</sub>-O]<sub>20</sub>-CH<sub>3</sub>) were homogeneously grafted via the sulfur bond to the inner surface of gold nanopore of 4.0 nm radii using the polyGraft Program.<sup>40</sup> The PEO chain length, grafting density of 0.46 nm<sup>-2</sup> and the pore size were selected to obtain an overlapping mushroom grafted chain conformation or a weak brush<sup>34</sup> that would be more susceptible to conformational changes and therefore more relevant for the study of

nanopore gating. Cosolvents were added to the PEO-grafted nanopore system using Gromacs embedded module (*gmx insert-molecules*) by specifying the number of molecules to add, (listed in Table S1 of the Supporting Information) based on which the volume of cosolvent was calculated.

The SPC/E model<sup>41</sup> was used for water, and the modified OPLS-AA force field was employed for PEO chains, as in our previous PEO-grafted gold nanopore paper.<sup>34</sup> For the cosolvent, the standard OPLS-AA<sup>42</sup> parameters were used for ethanol, acetic acid (ATA), and isobutyric acid (IBA). Modified OPLS-AA parameters were used for tetrahydrofuran (THF)<sup>16</sup> and butanol<sup>43</sup> which have been shown to better reproduce the solution properties. The geometric mixing rule was used for unlike pair interaction.

All systems were firstly energy minimized followed by 10 ns of NVT equilibration at 300 K using the Berendsen thermostat and 10 ns of NPT equilibration at 300 K and 1 bar pressure using the Berendsen thermostat and the Berendsen barostat. All production run NPT simulations were carried out for 100 ns at 300 K and 1 bar pressure using the V-rescale thermostat (time constant of 0.1 ps) and Berendsen barostat (time constant of 5.0 ps). For short-ranged pair and electrostatic interactions, a 1.0 nm cut-off distance was used with long-range electrostatic interactions calculated using the PME method. Long-range corrections for pair interactions were applied for the pressure and energy. All chemical bonds connected with hydrogen atoms were constrained using the LINCS algorithm to enable a time step of 2 fs. The equation of motion was evolved using the leapfrog algorithm with periodic boundary conditions in all directions.

For data analysis, such as PEO/water/cosolvent volume fraction and hydrogen bond distribution, the positions of atoms within cylindrical shells of 0.4 nm width were analyzed starting from the pore surface to the center. For volume fraction analysis, 0.030 nm<sup>3</sup> was used for the water volume, 0.025 nm<sup>3</sup> for CH<sub>2</sub>, 0.035 nm<sup>3</sup> for CH<sub>3</sub>, 0.016 nm<sup>3</sup> for the oxygen of PEO, and 0.0184 nm<sup>3</sup> for the sulfur atom. Cosolvent volume fraction was obtained by subtracting the volume of PEO and water for each shell. For hydrogen bonding analysis (PEO with water/cosolvent), the following geometrical criteria were adopted: the distance between a hydrogen bond donor (D) and acceptor (A) is less than 0.35 nm ( $r_{DA} \le 0.35$  nm); and the angle between a hydrogen (H) atom bonded to a donor, the donor and the acceptor ( $\angle$ HDA) is less than 30° ( $\angle$ HDA  $\leq$  30°). For the PEO chain conformation analysis, we employed the Gromacs embedded module (gmx polystat). Statistical data analysis was performed on the final 5 ns of simulation trajectory with the data saved every 10 ps. The data plotted and discussed in the text are the time averages (and ensemble average for the radius of gyration and end-to-end distance) with the error bars calculated as a standard deviation, except for the diffusion coefficient data, where an ensemble average have been calculated.

#### RESULTS AND DISCUSSION

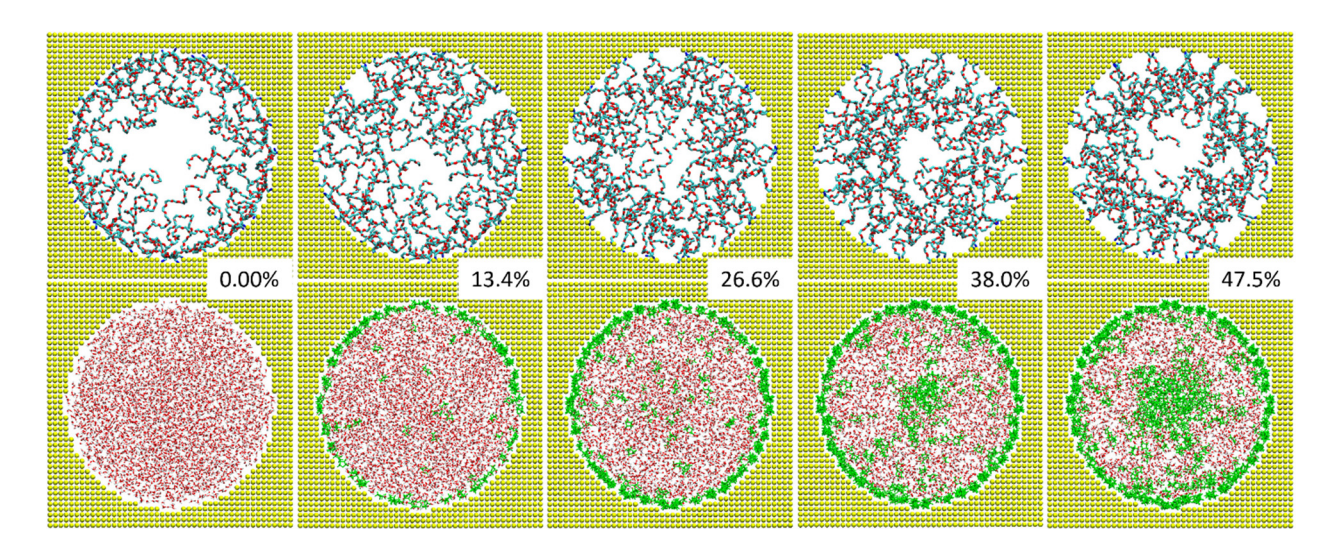


Figure 1. Cross-sectional MD simulation snapshots of PEO-grafted gold nanopore at different THF concentrations: 0.00%, 13.4%, 26.6%, 38.0%, 47.5% by volume from the left to the right. Gold nanopores are shown in yellow, PEO backbone (top panel) is shown in cyan (carbon atoms) and red (oxygen atoms); water (bottom panel) is shown in red (oxygens) and white (hydrogens), while THF (bottom panel) is shown in green. The nanopore radius is 4.0 nm, grafting density of PEO (of 20 repeat units) is 0.46 nm<sup>-2</sup>.

The equilibrated structure of PEO- grafted gold nanopore (4nm in radius) solvated by water is shown in the left column of Figure 1 for grafting density 0.46 nm<sup>-2</sup> and represents our reference system. As is seen, the PEO chains assume an overlapping mushroom-like conformation with an average radius of gyration 0.92 nm and are partially adsorbed on the nanopore surface, replacing water.<sup>34</sup> Using this reference system, we investigate the change of PEO conformation and distribution of polymer and solvent(s) within the nanopore upon addition of different cosolvents.

**THF addition.** THF is water soluble and a proton acceptor, just like PEO, and is a good solvent for PEO. Figure 1 shows that upon initial THF addition it tends to adsorb on the gold nanopore surface, as is seen in Figure 1, where the morphology of the PEO layer and

water/THF distribution within the nanopore are shown at various THF concentrations. THF adsorption on the gold surface occurs at all concentrations studied and is consistent with previous experimental observations of adsorption of liquid THF on a gold surface<sup>44</sup> and our previous observations for planar PEO-grafted gold surfaces. 16 The origin of the effect is in replacement of adsorbed PEO and water at the nanopore surface. Accordingly, PEO extends towards the nanopore center resulting effectively in nanopore closure. Indeed, upon an increase of THF concentration in solution its volume fraction near the pore surface increased reaching about 0.75 volume faction, while the corresponding volume fractions of PEO and water decreased from 0.65 to 0.2 and 0.3 to 0.05, respectively, as shown in Figure 2. As PEO desorbs from the nanopore surface its volume fraction in the middle of the nanopore increases from 0 to 0.1, while the water fraction decreases to about 0.6 at the THF volume fraction of 0.3. Interestingly, THF is mostly excluded from the PEO layer (Figure 1, Figure 2), where the PEO volume fraction reaches 0.4 surrounded by water. A similar observation has been made previously by one of us for a planar PEO-grafted gold surface, 16 for a higher polymer grafting density and larger fraction of THF in solution (80 vol%). Because THF competes with PEO for hydrogen bonding with water, exclusion from the PEO layer ensures good solvation of THF. Further addition of THF results in its saturation at the nanopore surface and the excess THF starts to concentrate at the center of the nanopore, driving away PEO together with some water (Figure 2). As a result, PEO assumes a more compact conformation concentrating in the middle area between the nanopore surface and nanopore center and resulting in reopening the nanopore (Figure 1, Figure 2).

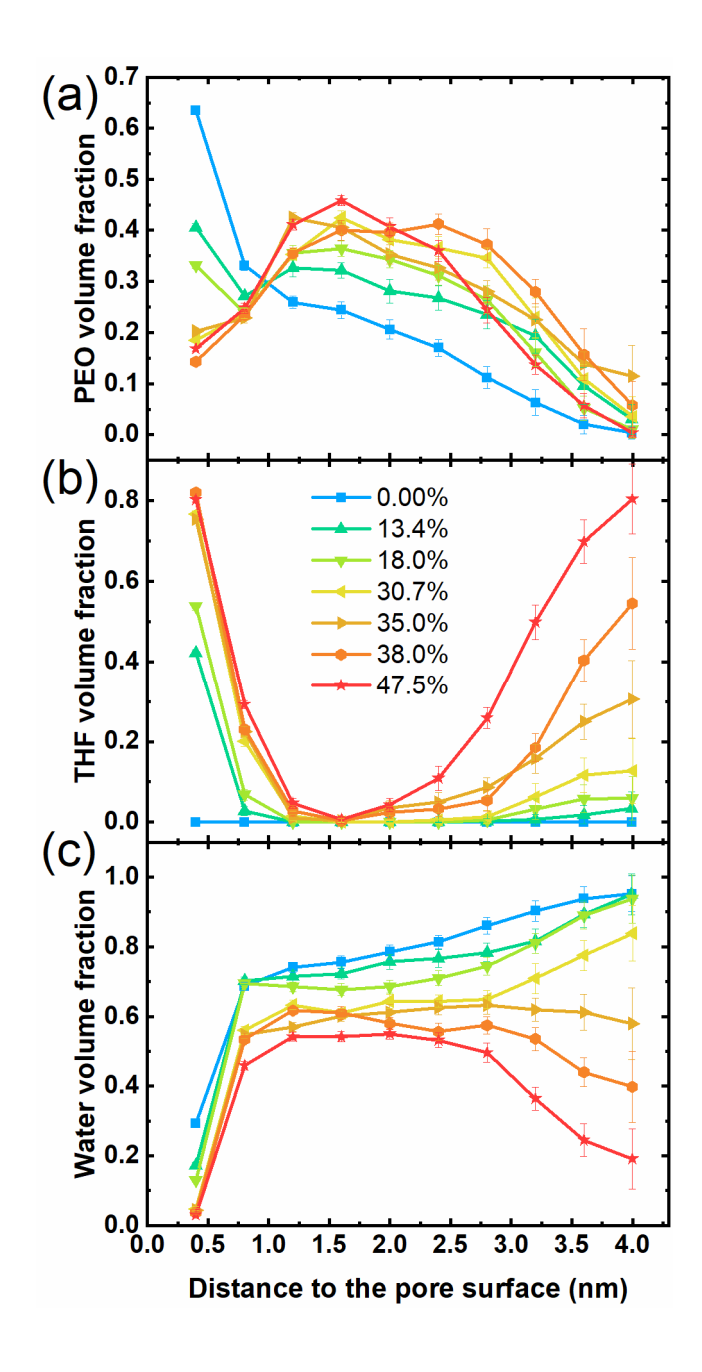


Figure 2. PEO (a), THF (b), and water (c) volume fractions as functions of the distance to the pore surface at different total volume fraction of THF:0 squares, 0.134 up triangles, 0.18 down triangles, 0.3 left triangles, 0.35 right triangles, 0.38 circles and 0.475 stars.

To characterize numerically the nanopore open/closed states, i.e. gating capability, we quantified the PEO layer thickness, or height (H):<sup>34</sup>

$$H = 3 \frac{\int_0^R (R - r) \Phi(r) r^2 dr}{\int_0^R \Phi(r) r dr}$$
 (1)

where  $\Phi(r)$  is the volume fraction of PEO at a radial distance r from the pore center shown in Figure 2a, and R=4 nm is the radius of the nanopore. We note that Eq. (1) takes into account the curvature effect of the cylindrical nanopore and the coefficient 3 originates from the normalization of the layer height for a constant polymer density. The change of the polymer layer height as a function of the THF concentration is shown in Figure 3. One can see that the brush height firstly increases from about 2.4 nm (without THF) to about the radius of the pore ( $H \approx R = 4.0$  nm) at intermediate THF concentration (30% by volume), which corresponds to nanopore closing and at higher THF concentration the height is decreased, consistent with reopening of the nanopore. The layer thickness change is essentially caused by the conformation change of PEO, e.g., the radius of gyration ( $R_g$ ) or the end-to-end distance  $R_{\rm end}$  change, as is shown in Figure S1 of the Supporting Information, which also firstly increase (when PEO is desorbed and extended to the pore center) and then decrease (when PEO is pushed back due to aggregation of THF).

In summary, THF addition firstly causes PEO desorption from the nanopore surface and extension towards the nanopore center effectively leading to nanopore closure. When the nanopore surface is saturated by THF, the excess resides at the nanopore center compressing PEO layer and resulting in reopening of the nanopore.

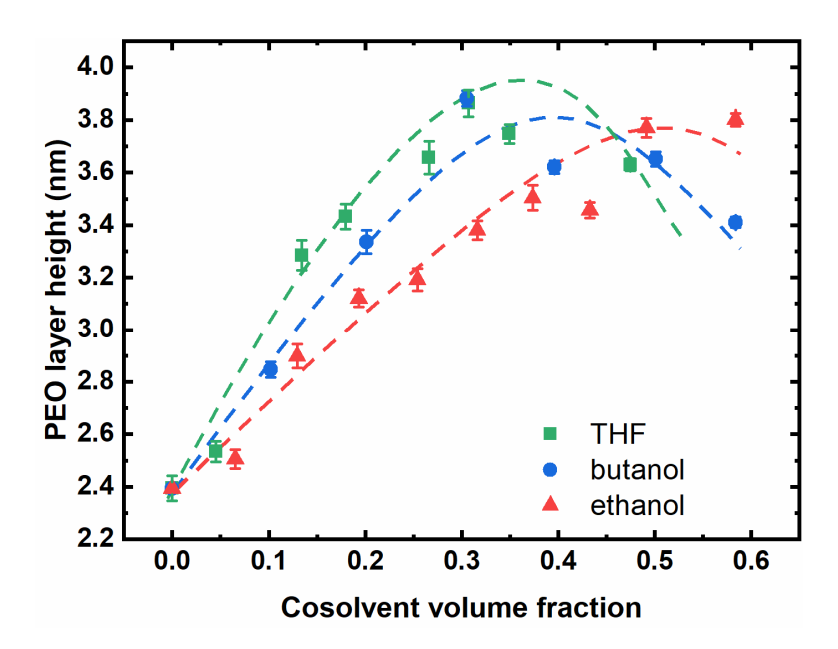


Figure 3. PEO layer height as a function of the cosolvent volume fraction for THF (green square), butanol (blue dot) and ethanol (red up-triangle). Dashed lines are guides for the eye. The nanopore radius is 4.0 nm, grafting density of PEO (of 20 repeat units) is 0.46 nm<sup>-2</sup>.

Ethanol and butanol addition. In contrast to THF which is a proton-acceptor, ethanol and butanol can also be proton donors and form hydrogen bonds both with water and PEO. Having different hydrophobicity due to the length of the aliphatic segment for ethanol and butanol (see Table S2 of the Supporting Information), it is interesting to compare the morphological changes of PEO layer and cosolvent distribution upon alcohol addition. Computer simulation snapshots of PEO-grafted nanopore at various alcohol concentrations are shown in Figure 4. One can see that, similar to THF, ethanol and butanol also adsorb onto the nanopore surface, replacing PEO which results in PEO extension towards the center, effectively closing the pore at some intermediate concentrations, ~ 40 volume % of butanol and 50 volume % of ethanol. The volume fraction of ethanol and butanol near the nanopore surface saturates as their concentration increases, as shown in Figure S2 of the Supporting Information, in a very similar manner as THF (Figure 2b). However, the distributions of

ethanol and butanol within the grafted PEO layer and near the nanopore center are very different, as is seen in the snapshots presented in Figure 4. Compared to butanol, ethanol is more homogeneously distributed in the PEO layer as it readily forms hydrogen bonds with PEO (Figure 5). Only at high ethanol concentrations does ethanol start to aggregate near the nanopore center of the pore while maintaining its presence within the PEO layer. In contrast, the more hydrophobic butanol resides primarily at the nanopore surface and in the center and has a minimal presence within the PEO layer where it forms very few hydrogen bonds (Figure 5). With an increase of butanol concentration, it saturates near the nanopore surface and strongly aggregates at the nanopore center like THF. Accordingly, PEO firstly desorbs from the nanopore surface closing the nanopore and with an increase of butanol content at the center, PEO layer becomes compressed, reopening the pore in a manner very similar to THF.

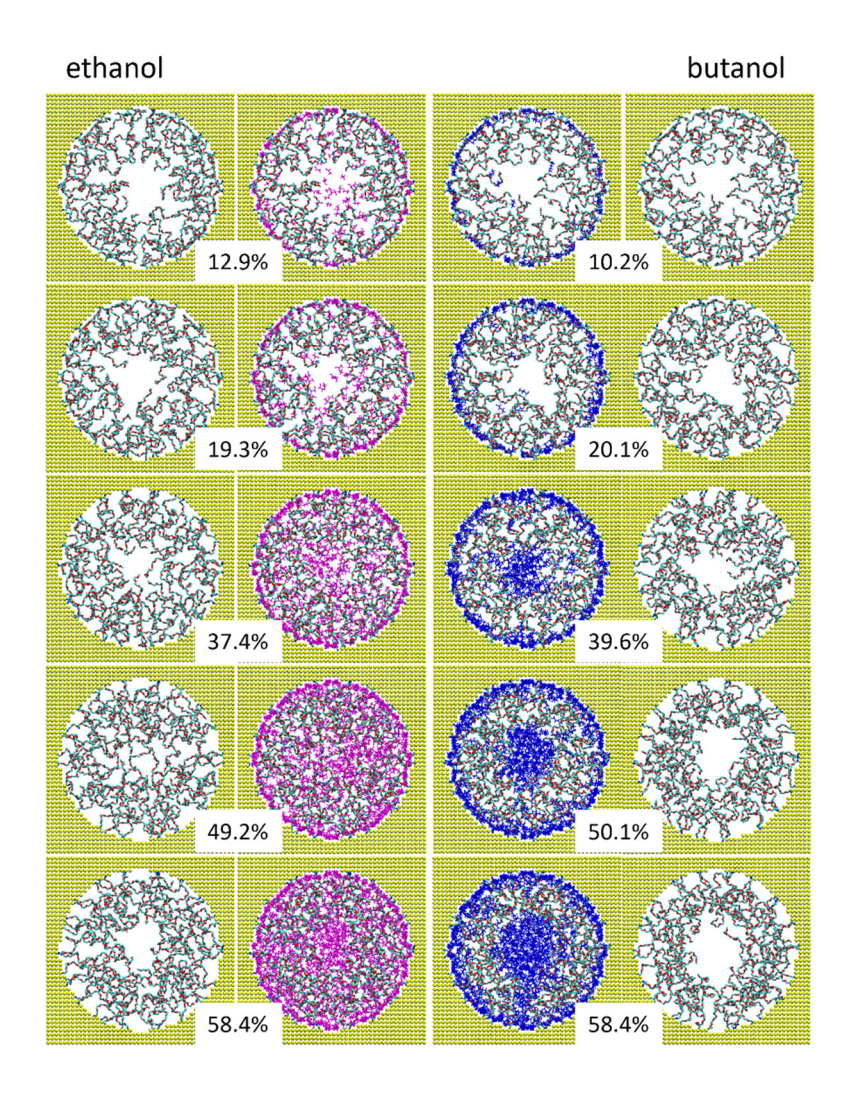


Figure 4. Cross-sectional MD simulation snapshots of PEO-grafted gold nanopore in mixed ethanol/water (left two panels) and butanol/water (right two panels) solutions at different cosolvent content (by volume, low to high from the top to the bottom). Gold nanopores are shown in yellow, PEO backbone is shown in cyan (carbon atoms) and red (oxygen atoms), ethanol and butanol are shown in magenta and blue, respectively.

The PEO layer height in the presence of ethanol and butanol are shown in Figure 3 in comparison to that for THF (see eq.1). The PEO layer height firstly increases with the cosolvent concentration at a higher rate for butanol and THF than for ethanol (Figure 3) due to the differences of their interactions with PEO (ethanol better solvates PEO than butanol or THF). The PEO layer height reaches a maximum corresponding to pore closure at about

40% by volume for butanol and at about 50% of ethanol, which exhibits a weaker nanopore-closing. At higher butanol content its aggregation at the nanopore center results in reopening of the nanopore similar to THF. This behavior is reflected in the radius of gyration and end-to-end distance changes of PEO, shown in Figure S1 of the Supporting Information.

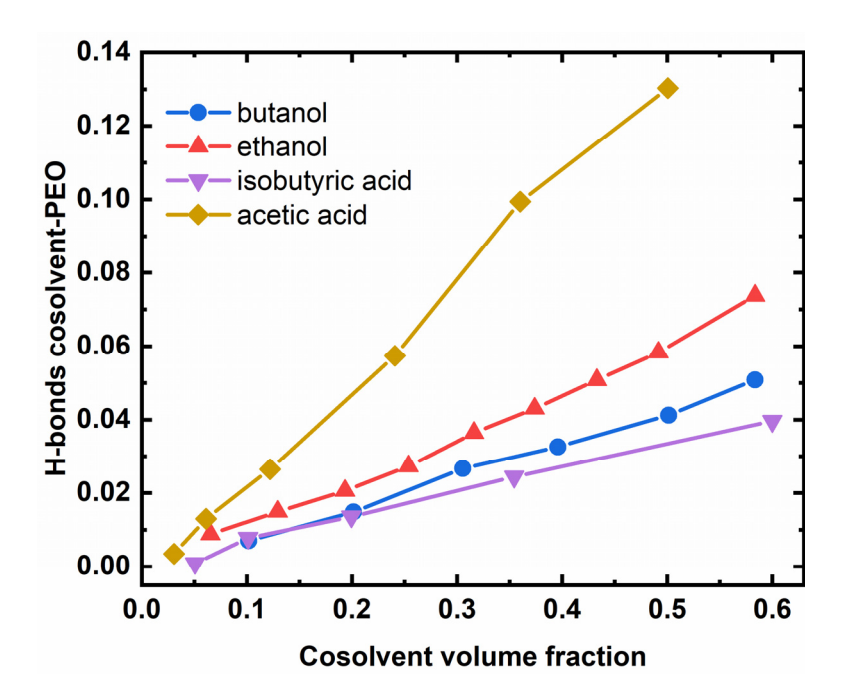


Figure 5: The average number of hydrogen bonds between cosolvent and PEO per repeat unit of PEO as functions of cosolvent volume fraction. Error bars are smaller than the symbol size.

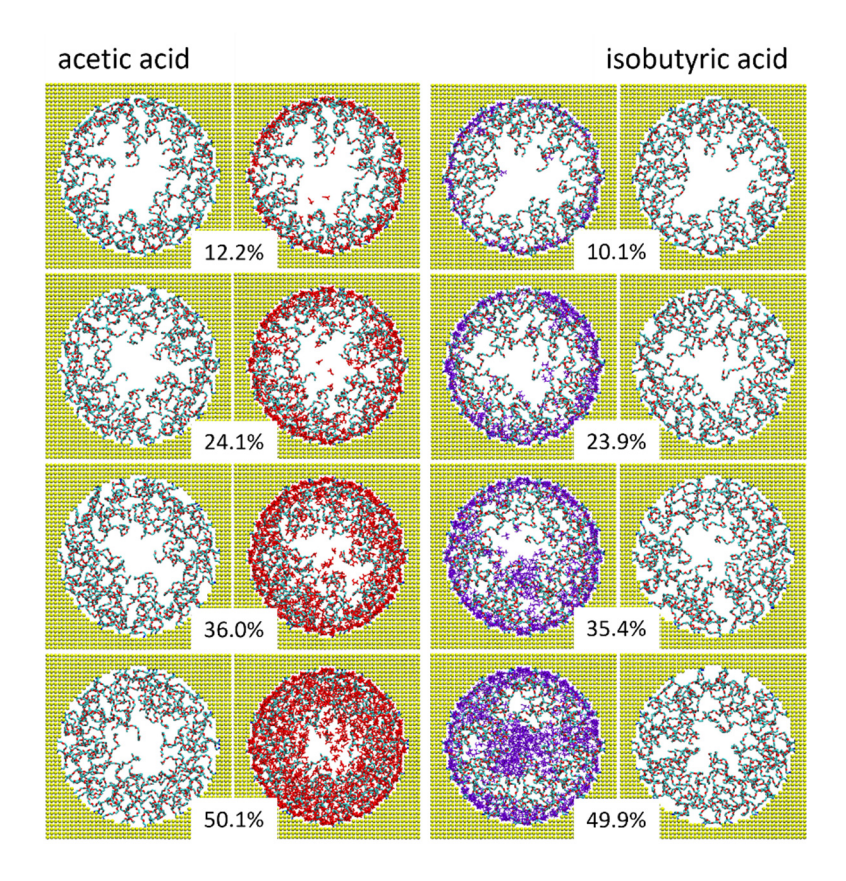


Figure 6. Cross-sectional MD simulation snapshots of PEO-grafted gold nanopore in mixed acetic acid (ATA)/water (left two panels) and isobutyric acid (IBA)/water (right two panels) solutions at different cosolvent content (by volume, low to high from the top to the bottom). Gold nanopores are shown in yellow, PEO backbone is shown in cyan (carbon atoms) and red (oxygen atoms), ATA and IBA are shown in red and violet, respectively.

ATA and IBA addition. Similar to ethanol and butanol, acetic acid (ATA) and isobutyric acid (IBA) can also form hydrogen bonds with water and PEO, but via the carboxylic group. We compared the morphological changes of PEO layers upon addition of ATA and IBA and cosolvent distribution within the nanopore at different concentrations as shown in Figure 6. As is seen, similar to the other cosolvents discussed above, ATA and IBA are also absorbed to the gold surface. What is more striking and different from other cosolvents discussed above, is that the PEO layer shrinks upon addition of a small amount (about 5% by volume) of IBA and ATA effectively opening the pore, as indicated by the change of the PEO volume

fraction distribution shown in Figure S3 of the Supporting Information. The PEO volume fraction decreased closer to the pore center and increased within  $1\sim2$  nm of the pore surface. A similar effect has been reported by one of us for PEO (and polypropylene oxide, PPO) in mixed IBA/water solution<sup>36</sup> in the absence of confinement and originates from the partial decrease and exchange of PEO-water hydrogen bonds for IBA-PEO (or ATA-PEO) ones (cf. Figure 5 and Figure S4 of the Supporting Information). As the concentration of ATA or IBA increases, the ATA-PEO and IBA-PEO hydrogen bonds (including some bridges to water via =0) stabilize the PEO conformation and as a consequence the PEO layer extends to the pore center. At all concentrations, ATA preferentially resides homogenously within the PEO layer, while IBA firstly saturates the nanopore surface and then aggregates near the nanopore center at high concentrations (Figure 6 and Figure S3 of the Supporting Information). The difference in the behavior is due to the weaker hydrophobicity of ATA (Table S2 of the Supporting Information) and stronger tendency for hydrogen bonding with PEO compared to IBA. Consistent with the discussion above and the snapshots shown in Figure 6, the height of PEO layer firstly decreases upon addition of a small amount of IBA and especially ATA, opening the pore (Figure 7a). Accordingly, the radius of gyration of PEO decreases to a larger extent upon ATA addition compared to IBA, as shown in Figure 7b. Further addition of carboxylic acids results in a systematic increase of the radius of gyration and PEO layer height thereby reducing the gap at the center of the nanopore. The change of end-to-end distance of PEO shows a similar trend, as shown in Figure S5 of the Supporting Information.

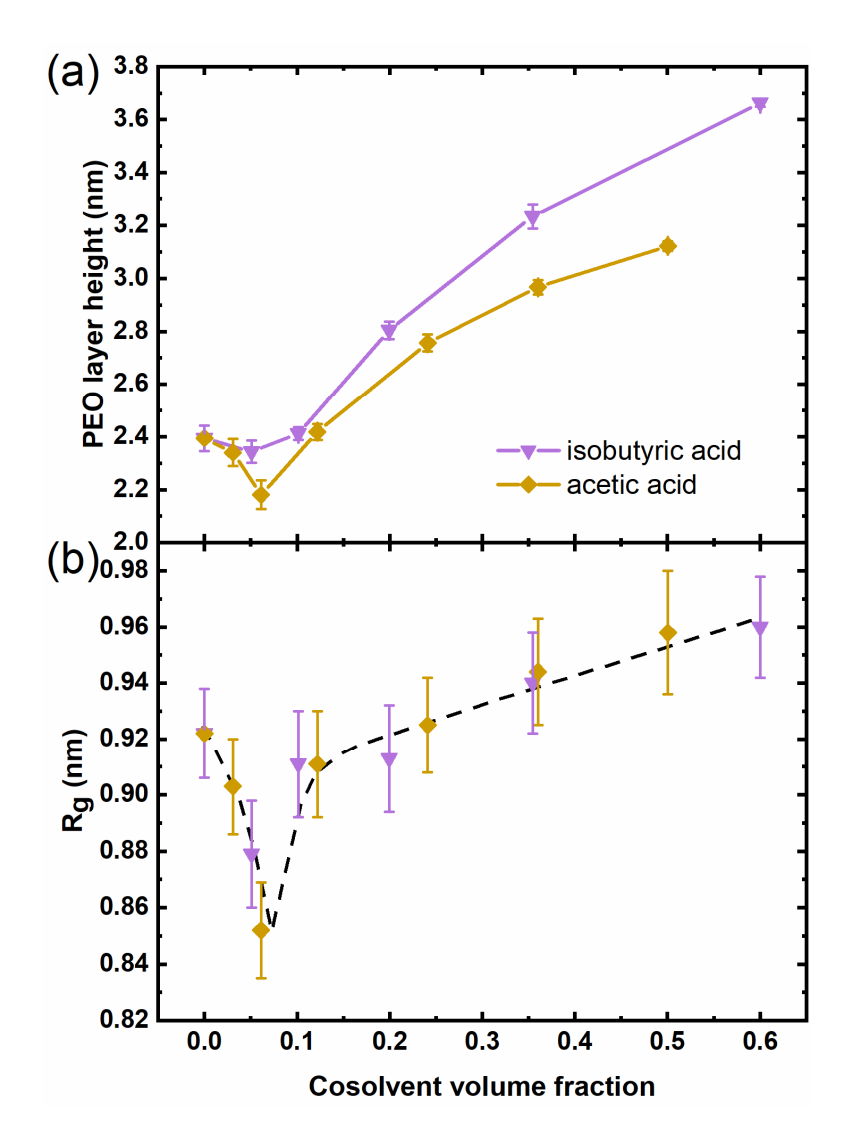


Figure 7. PEO layer height (a) and PEO radius of gyration (b) as a function of the IBA and ATA volume fraction. The black dashed line is a guide for the eye.

Comparison of cosolvent effects. To compare numerically the changes in cosolvent distribution within the nanopore for all studied cases, we show in Figure 8 the volume fractions of cosolvents within 0.4 nm of the nanopore surface and within 0.4 nm of nanopore center as functions of the total cosolvent volume fraction. As discussed above, all cosolvents adsorb at the nanopore surface. Initially the increase in the volume fraction of cosolvent adsorbed at the interface occurs for the most cosolvents in a linear matter  $\phi_{ads} \sim 4\phi_{cs}$ , where

φ<sub>cs</sub> is the total fraction of cosolvent within the nanopore, indicating a strong tendency to replace PEO and water at the nanopore surface. Ethanol adsorbs somewhat less strongly due to favorable interactions (hydrogen bonding) with water and PEO. When the cosolvent volume fraction at the surface reaches about 0.3-0.4 a bifurcation in cosolvent behavior appears. THF and butanol continue to populate the nanopore surface until reaching saturation at 0.8 volume fraction at the interface, which is reached between 0.3 to 0.4 total volume content of cosolvent in the nanopore. At higher cosolvent content the excess of THF and but anolis concentrated at the nanopore center. For the other three cosolvents, ethanol, acetic and isobutyric acids, adsorption at the interface slows after achieving  $\phi_{ads} \approx 0.4$ . Ethanol and especially acetic acid, having favorable hydrogen bonding interactions with PEO chains (Figure 5), spread more homogeneously throughout the polymer layer in addition to their presence at the interface. Isobutyric acid, while also forming some hydrogen bonds with PEO starts phase separating from water and forms a droplet near the nanopore center when its total volume content exceeds 0.3, similar to what has been observed in solution.<sup>36</sup> Overall, acetic and isobutyric acids saturate the nanopore surface at about 0.7 volume fraction, while ethanol reaches 0.8 surface volume fraction at about 0.5 total volume content. Acetic acid which forms the most hydrogen bonds with PEO among all cosolvents (Figure 5) has the smallest presence at the center on nanopore followed by the ethanol (Figure 8b).

In Figure 9a we compare the distribution of cosolvents and PEO as functions of the distance to the pore surface at the cosolvent content of 50% by volume. One can see that near the pore surface (within 1.0 nm), the differences are very small with a slightly smaller fraction of ATA and IBA, as discussed above. Within the polymer layer (1.0~2.5 nm from the surface), the volume fractions start to differ. As can be seen, the ATA volume fraction is the highest,

about 0.3, demonstrating stronger preference of ATA to reside within PEO layer compared to, e.g., ethanol (volume fraction 0.2). This is due to the stronger capability of ATA to form hydrogen bonds with PEO, as shown in Figure 5. The average number of hydrogen bonds formed per PEO oxygen with ATA is about 0.13 while twice smaller, 0.06, with ethanol. In contrast, IBA has a volume fraction of 0.1 in this region and THF/butanol even less, 0.05. Lastly, near the pore center (2.5~4.0 nm), ATA has a low volume fraction (0.05 in the pore center), as it prefers to reside within the PEO layer rather than in water. IBA, on the other hand, phase separates, with a high volume fraction of 0.85 in the pore center, similar to THF and is exceeded only by butanol. Consequently, in the presence of ATA and IBA the PEO volume fraction is higher near the pore surface (within 1.0nm of the surface), but is lower in the middle layer (1.0~2.5nm) than with other cosolvents, as shown in Figure 9b. Near the pore center (>2.5nm), the PEO volume fraction is the lowest and vanishes at pore center in the presence of ATA; while PEO volume fraction at the center is higher in the presence of IBA and especially ethanol.

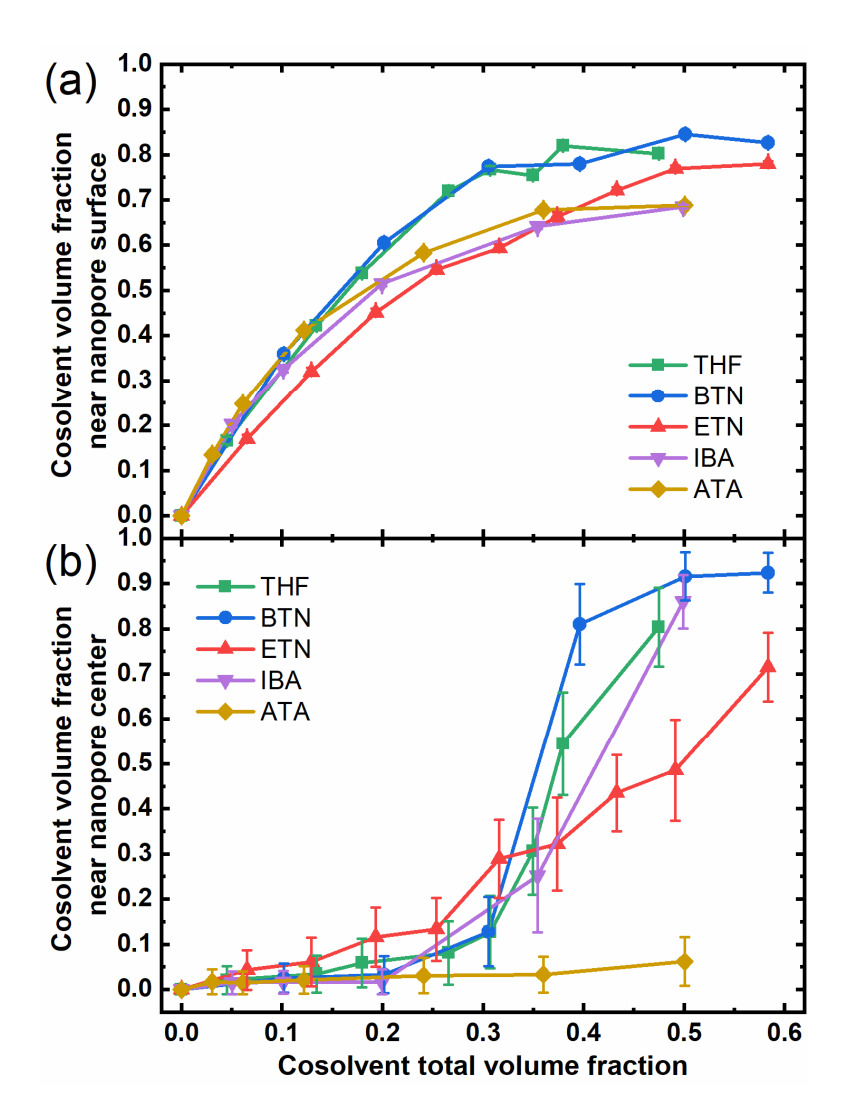


Figure 8: Cosolvent volume fraction near the pore surface (a) and near the pore center (b) for THF (green squares), butanol (blue circles), ethanol (red up-triangles), isobutyric acid (violet down-triangles), and acetic acid (yellow diamonds) as a function of cosolvent total volume fraction. Error bars in (a) are smaller than the symbol size.

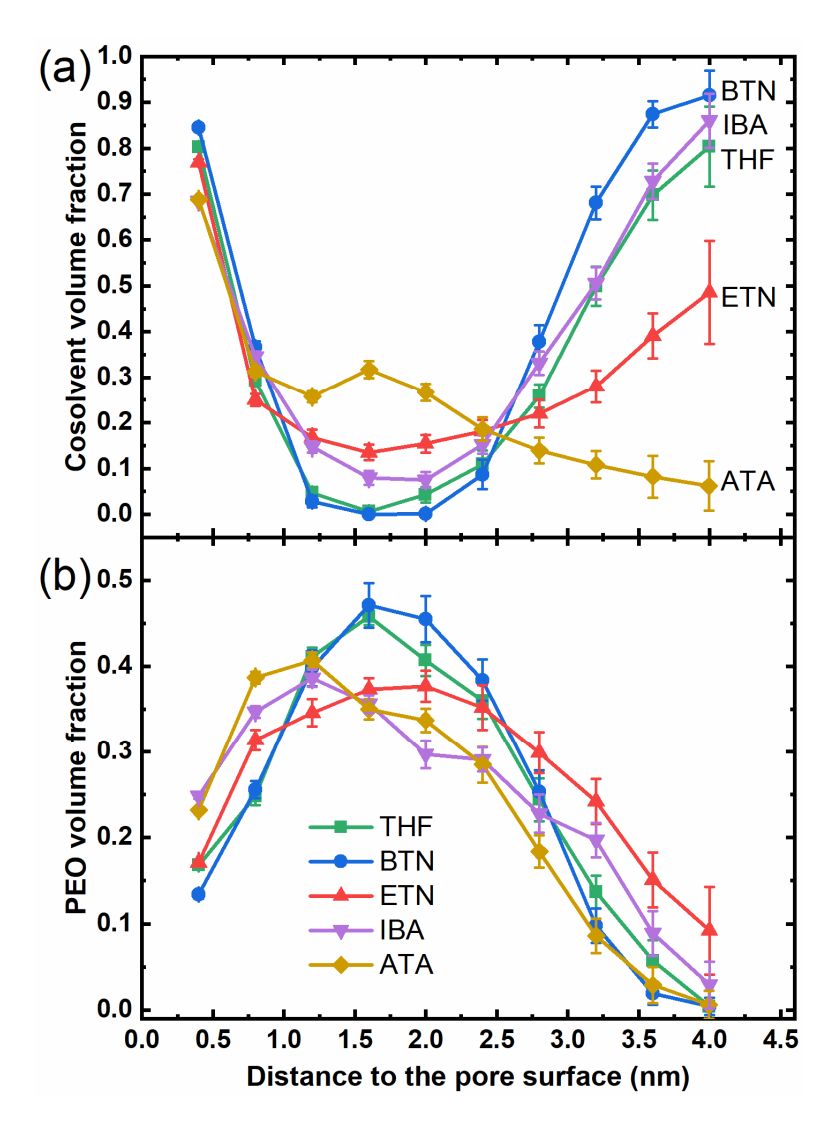


Figure 9: Cosolvent volume fraction (a) and PEO volume fraction (b) as functions of the distance to the nanopore surface at the cosolvent content of 50% by volume: THF (green squares), butanol (blue circles), ethanol (red up-triangles), isobutyric acid (violet downtriangles), and acetic acid (yellow diamonds).

To compare the gating capabilities of all cosolvents, we analyze in Figure 10 the size of the open pore region, estimated as the difference between the nanopore radius R and PEO layer height H (calculated using eq.1), R - H, as a function of the cosolvent concentration. As is seen, all cosolvents are capable of nanopore closure due to cosolvent adsorption and polymer desorption from the nanopore surface. At the same, only ATA and IBA can open a pore at low cosolvent content (~5% by volume) due to the interplay in carboxylic acid-PEO and water-PEO hydrogen bonding, while THF and butanol are capable of pore reopening at high concentrations (above 40% by volume) when cosolvent aggregation at the nanopore center occurs. While both IBA and butanol phase separate at high concentrations, the open pore size is larger with butanol than that with IBA, due to the presence of IBA within the PEO layer while butanol is mostly excluded from it, as discussed above. On the other hand, for nanopore closure a high concentration of ATA, IBA or ethanol is needed, while in contrast only an intermediate concentration of THF or butanol is required. It is important to note that the maximum PEO layer height and minimum of nanopore opening occurs at the cosolvent content at which saturation of cosolvent at the nanopore surface is achieved and the excess of cosolvent starts to accumulate at the nanopore center (Figure S6). For THF and butanol this happens at the overall cosolvent volume fraction of about 0.30-0.35, while for ethanol, ATA or IBA only at about 0.50 cosolvent volume fraction. One important insight from Figure 10 is the interaction strength between cosolvent and PEO can be ranked as follows: THF < butanol < ethanol/IBA < ATA.

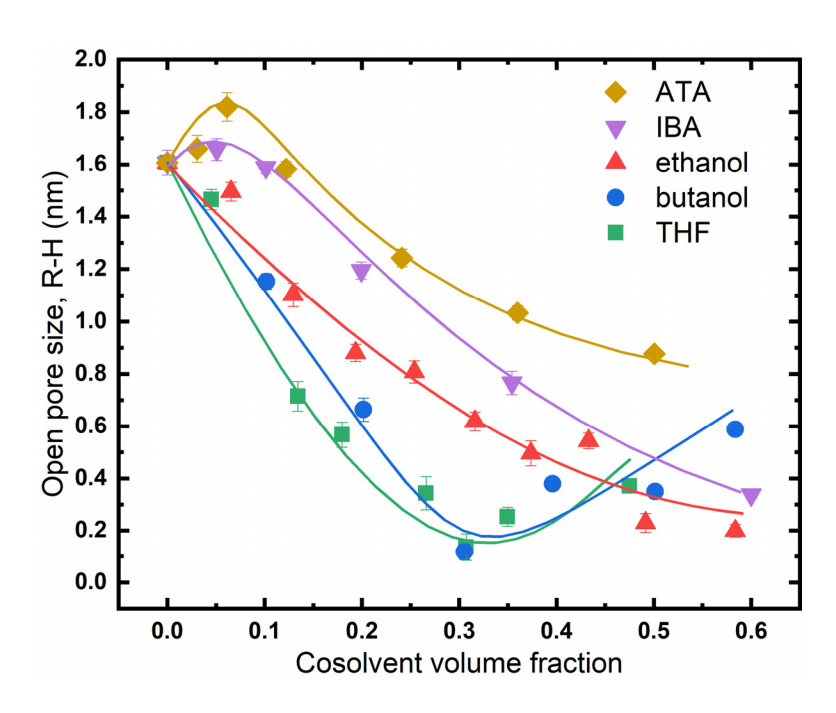


Figure 10. The open pore size (R-H) as a function of the cosolvent volume fraction for all cosolvents. Lines are guides for the eye.

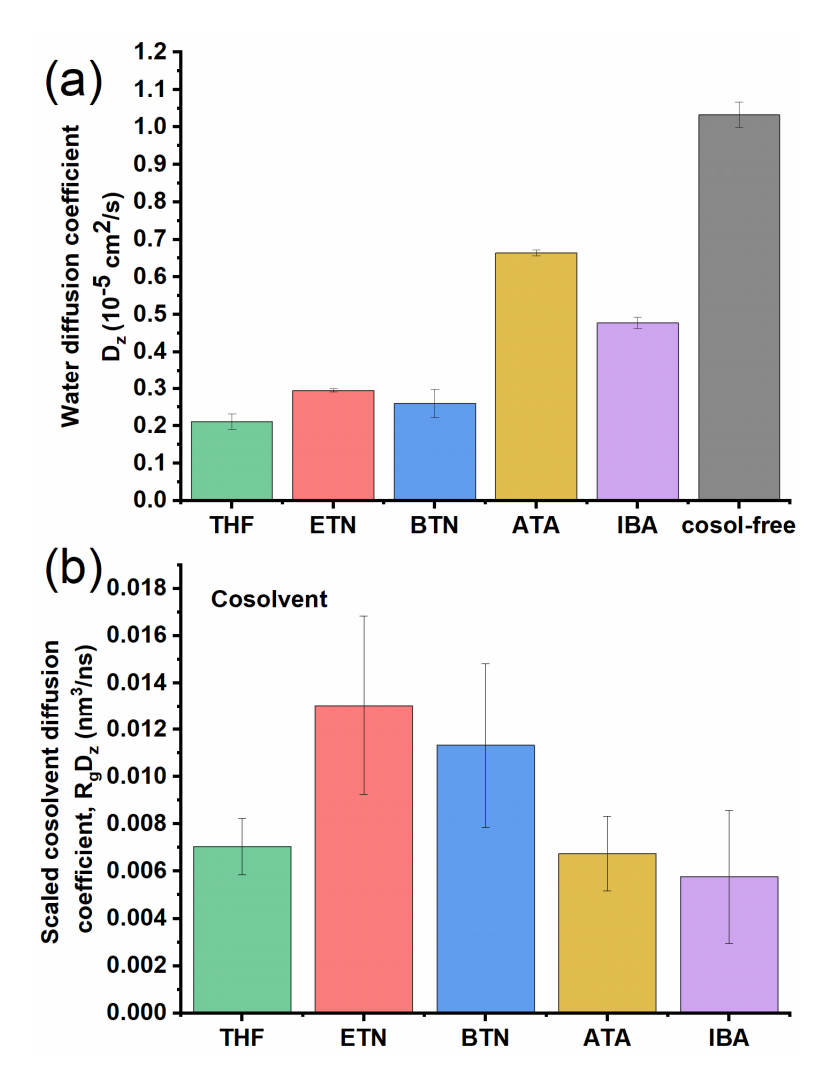


Figure 11. The diffusion coefficient of water,  $D_z$  (a) and the scaled cosolvent diffusion coefficient ( $R_aD_z$ ) (b) at the concentration of 0.35 by volume and T=300K.

**Solvent Diffusion.** While the above analysis of the structure of PEO layer, water and cosolvent distribution provides detailed information on the interactions between PEO, water, cosolvent, and gold surface, we have not discussed yet the solvent dynamics, which is important for practical applications of nanopore-containing materials. To characterize this property, we calculated the lateral diffusion coefficient ( $D_z$ ) along the nanopore long axis based on the mean square displacement (MSD):

$$MSD(t) = \langle |z_i(t) - z_i(0)|^2 \rangle = \frac{1}{N} \sum_{i=1}^{N} |z_i(t) - z_i(0)|^2 = 2D_z t$$
 (2)

where  $z_i$  is the location of an atom and N is the total number of atoms for that type. The lateral diffusion coefficient  $(D_z)$  can then be obtained from the MSD(t) curve. We note that the calculation is done for all cosolvent or water molecules within the nanopore and represents the ensemble average, while the solvent dynamics could be very different in different regions of nanopore, *e.g.*, very slow diffusion is expected for solvent molecules adsorbed on the nanopore surface compared to the pore center.

The lateral diffusion coefficient for water molecules  $D_z$  is shown in Figure 11a at an intermediate cosolvent concentration of 35% by volume. One can see that the lateral diffusion of water in the presence of cosolvents is slowed down in all cases compared to that for the reference PEO-grafted nanopore in water (without cosolvent) which is about 1.03  $(10^{-5} \text{cm}^2/\text{s})$ . As a reference, SPC/E water diffusion coefficient in the bulk is about  $2.6 \sim 3.18$ (10-5cm<sup>2</sup>/s).<sup>45</sup> Slowing down the water diffusion can be expected due to the increased viscosity of the cosolvent. On the other hand, some fraction of water was adsorbed to the nanopore surface its release can increase the average diffusivity of water. Comparing different mixed solvents, the diffusion of water in IBA or ATA aqueous solution is relatively faster (about two-fold) than that in ethanol, or butanol mixed solution, which in turn is slightly faster than that in THF/water mixed solution (Figure 11a). These differences are attributed to the degree of the pore opening (Figure 10). For example, in ATA/water and IBA/water mixed solvents the opening is the largest and water experiences the least obstruction. In addition, IBA, ethanol and especially ATA release more water from interactions with PEO, while for THF and butanol hydrogen bonding between water and PEO

is only weakly affected by the cosolvent (Figure S4). In contrast, the stability of hydrogen bonding between water and cosolvent (Figure S7 of the Supporting Information) seems to have less impact on the water dynamics but may influence the cosolvent diffusion.

We calculated the lateral diffusion coefficient of all cosolvents at the same solvent composition (0.35 cosolvent volume fraction), as shown in Table S3 of the Supporting Information. Since cosolvent molecules have different sizes, it is worthwhile to compare diffusion coefficients scaled by their radius of gyration, i.e. obtained by multiplying the diffusion coefficient, derived from Eq. (2), by the radius of gyration of the cosolvent Rg using the Stocks-Einstein relation, i.e. D<sub>z</sub>R<sub>g</sub> as shown in Figure 11b. One can see that the scaled diffusion coefficient of ethanol and butanol is higher (two-fold) than that for THF, IBA and ATA. Water forms more stable hydrogen bonds with carboxylic acids than alcohols (Figure S7 of the Supporting Information) and that can be a factor in the observed slower diffusion of ATA and IBA. At the same time, the stability of water hydrogen bonded to THF is the lowest among cosolvents, so hydrogen bonding between water and THF is not the main factor in the results shown in Figure 11b. According to Figure 8, at this solvent composition there is a considerable fraction of alcohol present in the open pore region, while the carboxylic acids are mainly located within the PEO layer region (due to favorable hydrogen bonding) and THF-containing nanopore has a minimal pore opening. Therefore, both, the state of the pore opening and interaction of cosolvents with water and PEO layer affect the lateral diffusion of solvents, which is another important property to take into consideration while designing nanopore-containing materials for practical applications.

#### **CONCLUSIONS**

In summary, using atomistic molecular dynamics simulations we have elucidated the effects of cosolvent addition on the morphological change in PEO grafted gold nanopores, understanding of which is essential for nanopore gating control.

We have found that all cosolvents initially adsorb onto the nanopore surface (Figure 1, Figure 4, and Figure 6) in a similar manner, thereby releasing water and adsorbed PEO segments. With an increase of cosolvent content, THF and butanol continue to strongly adsorb onto the nanopore surface reaching 0.8 volume fraction at saturation, while ATA and IBA have a slightly lower saturation volume fraction of 0.7. Further away from the pore surface  $(1.0\sim2.5\text{nm})$  but still within the PEO layer (Figure 8 and Figure 9), there is a considerable amount of ATA (reaching a volume fraction of 0.3), and a somewhat smaller presence of ethanol ( $\sim$ 0.2 volume fraction) and IBA ( $\sim$ 0.1 volume fraction). On the other hand, butanol and THF are practically excluded from the PEO layer. This difference in cosolvent population within the PEO layer is related to their capability for hydrogen bond formation with PEO (Figure 5), as well as the strength of the cosolvent-water interactions. Indeed, acetic acid and ethanol both form more hydrogen bonds with PEO than other cosolvents, but also hydrogen bond with water and are distributed more homogeneously throughout the nanopore (Figure 5, Figure 8). In contrast butanol and isobutyric acid form a smaller number of hydrogen bonds with PEO and phase separate from water at high cosolvent content and aggregate at the center of the nanopore. THF competes with PEO for hydrogen bonds with water and therefore becomes concentrated in the water-rich region near the pore center.

The presence of cosolvents also changes the PEO conformation. In all cases, adsorption of cosolvents at the nanopore surface results in PEO desorption and increases the thickness of PEO layer such that the PEO chains extend towards the pore center. (Figure 2, Figure S6 of the Supporting Information). When the cosolvent adsorption at the nanopore surface reaches saturation, the PEO layer thickness approaches a maximum and can result in nanopore closure. For THF and butanol this occurs at about 0.3-0.35 volume fraction, while ethanol, IBA and ATA reach the adsorption saturation limit only at a high volume fraction when the PEO layer expands, thereby reducing the polymer-free zone at the nanopore center (Figure 10). At high volume fractions THF and butanol, aggregate in the nanopore center compressing PEO layer and re-opening of the nanopore. In contrast, addition of a very small amount of IBA or ATA causes shrinking of the PEO layer and opening of the pore due to the change in solvation and redistribution of water-PEO, carboxylic acid-PEO hydrogen bonding.<sup>36</sup> With a further increase in ATA or IBA content the carboxylic acid-PEO hydrogen bonding becomes more prominent leading to PEO expansion along with desorption from the surface and closing of the nanopore (Figure 10).

Therefore, the nanopore gating capability of a cosolvent depends on its interactions with PEO and water (Figure 10) and can follow different scenarios. ATA and IBA are able to open the nanopore at low concentration through interactions with PEO and redistribution of hydrogen bonding (solvation changes). In contrast, butanol, and THF have minimal interactions with PEO and are capable of opening the nanopore at high concentrations due to the cosolvent aggregation in the nanopore center.

The abovementioned structural properties also affect the dynamics of water and cosolvents within the nanopore (Figure 11), which is relevant for regulating material transport or

translocation through polymer-grafted nanopores. Lateral water diffusion along the nanopore is mainly controlled by the size of the open region in the pore center (polymer-free), where the least obstruction is experienced. Therefore, a cosolvent that is able to open the pore can also speed up water diffusion. Cosolvent dynamics, on the other hand, are also affected by their interactions with PEO and water. ATA and IBA can form more stable hydrogen bonds with PEO than ethanol and butanol, thereby slowing down their dynamics. In general, both the state of the pore opening and interaction between cosolvents and PEO layer affect the lateral diffusion of solvents, which is important to take into consideration while designing nanopore-containing materials. Our insights on cosolvent distribution within the nanopore and cosolvent-initiated structural changes of a PEO layer provide guidance for the selection of cosolvents in the design of cosolvent-induced gated control devices based on a polymer-grafted nanopore system.

#### ASSOCIATED CONTENT

hydrogen bonded water to cosolvent as a function of time; the diffusion coefficient and radius of gyration of cosolvents at the concentration of 0.35 by volume.

#### **AUTHOR INFORMATION**

### **Corresponding Author:**

**Elena E. Dormidontova** – Polymer Program, Institute of Materials Science and Physics Department, University of Connecticut, Storrs, Connecticut 06269, United States. Orcid: 0000-0002-7669-8957. Email: elena@uconn.edu

#### **ACKNOWLEDGMENTS**

This research is supported by the National Science Foundation under Grant No. DMR-1916864. This work used the Extreme Science and Engineering Discovery Environment (XSEDE) through allocation TG-MAT210004 (supported by National Science Foundation grant number ACI-1548562) and the Advanced Cyberinfrastructure Coordination Ecosystem: Services & Support (ACCESS) program, which is supported by the National Science Foundation grants #2138259, #2138286, #2138307, #2137603, and #2138296.

#### REFERENCES

- (1) Pardehkhorram, R.; Andrieu-Brunsen, A. Pushing the Limits of Nanopore Transport Performance by Polymer Functionalization. *Chem. Commun.* **2022**, *58* (34), 5188–5204, DOI 10.1039/d2cc01164f.
- (2) Zhu, Y.; Gao, S.; Hu, L.; Jin, J. Thermoresponsive Ultrathin Membranes with Precisely Tuned Nanopores for High-Flux Separation. *ACS Appl. Mater. Interfaces* **2016**, *8* (21), 13607–13614, DOI 10.1021/acsami.6b03389.
- (3) Barsbay, M.; Güven, O.; Bessbousse, H.; Wade, T. L.; Beuneu, F.; Clochard, M. C.

- Nanopore Size Tuning of Polymeric Membranes Using the RAFT-Mediated Radical Polymerization. *J. Memb. Sci.* **2013**, *445*, 135–145, DOI 10.1016/j.memsci.2013.05.029.
- (4) Lee, H. S.; Penn, L. S. Polymer Brushes Make Nanopore Filter Membranes Size Selective to Dissolved Polymers. *Macromolecules* **2010**, *43* (1), 565–567, DOI 10.1021/ma9019569.
- (5) Ma, T.; Walko, M.; Lepoitevin, M.; Janot, J. M.; Balanzat, E.; Kocer, A.; Balme, S. Combining Light-Gated and PH-Responsive Nanopore Based on PEG-Spiropyran Functionalization. *Adv. Mater. Interfaces* **2018**, *5* (2), 1–9, DOI 10.1002/admi.201701051.
- (6) Buchsbaum, S. F.; Nguyen, G.; Howorka, S.; Siwy, Z. S. DNA-Modified Polymer Pores Allow PH- and Voltage-Gated Control of Channel Flux. *J. Am. Chem. Soc.* **2014**, *136* (28), 9902–9905, DOI 10.1021/ja505302q.
- (7) Zhao, Y.; Janot, J.-M.; Balanzat, E.; Balme, S. Mimicking PH-Gated Ionic Channels by Polyelectrolyte Complex Confinement Inside a Single Nanopore. *Langmuir* **2017**, *33* (14), 3484–3490, DOI 10.1021/acs.langmuir.7b00377.
- (8) Huang, K.; Szleifer, I. Design of Multifunctional Nanogate in Response to Multiple External Stimuli Using Amphiphilic Diblock Copolymer. *J. Am. Chem. Soc.* **2017**, *139* (18), 6422–6430, DOI 10.1021/jacs.7b02057.
- (9) Alem, H.; Duwez, A. S.; Lussis, P.; Lipnik, P.; Jonas, A. M.; Demoustier-Champagne, S. Microstructure and Thermo-Responsive Behavior of Poly(N-Isopropylacrylamide) Brushes Grafted in Nanopores of Track-Etched Membranes. *J. Memb. Sci.* **2008**, *308* (1–2), 75–86, DOI 10.1016/j.memsci.2007.09.036.
- (10) Lokuge, I.; Wang, X.; Bohn, P. W. Temperature-Controlled Flow Switching in Nanocapillary Array Membranes Mediated by Poly(N-Isopropylacrylamide) Polymer Brushes Grafted by Atom Transfer Radical Polymerization. *Langmuir* **2007**, *23* (1), 305–311, DOI 10.1021/la060813m.
- (11) Budkov, Y. A.; Kolesnikov, A. L.; Georgi, N.; Kiselev, M. G. A Statistical Theory of Cosolvent-Induced Coil-Globule Transitions in Dilute Polymer Solution. *J. Chem. Phys.* **2014**, *141* (1), DOI 10.1063/1.4884958.
- (12) Mukherji, D.; Marques, C. M.; Kremer, K. Polymer Collapse in Miscible Good Solvents Is a Generic Phenomenon Driven by Preferential Adsorption. *Nat. Commun.* **2014**, *5* (1), 4882, DOI 10.1038/ncomms5882.
- (13) Bharadwaj, S.; Nayar, D.; Dalgicdir, C.; Van Der Vegt, N. F. A. An Interplay of Excluded-Volume and Polymer-(Co)Solvent Attractive Interactions Regulates Polymer Collapse in Mixed Solvents. *J. Chem. Phys.* **2021**, *154* (13), 134903, DOI 10.1063/5.0046746.
- (14) Bharadwaj, S.; Niebuur, B. J.; Nothdurft, K.; Richtering, W.; van der Vegt, N. F. A.; Papadakis, C. M. Cononsolvency of Thermoresponsive Polymers: Where We Are Now and Where We Are Going. *Soft Matter* **2022**, *18* (15), 2884–2909, DOI

- 10.1039/d2sm00146b.
- (15) Marko, J. F. Polymer Brush in Contact with a Mixture of Solvents. *Macromolecules* **1993**, 26 (2), 313–319, DOI 10.1021/ma00054a010.
- (16) Dahal, U. R.; Wang, Z.; Dormidontova, E. E. Hydration and Mobility of Poly(Ethylene Oxide) Brushes. *Macromolecules* **2017**, *50* (17), 6722–6732, DOI 10.1021/acs.macromol.7b01369.
- (17) Park, G.; Jung, Y. Many-Chain Effects on the Co-Nonsolvency of Polymer Brushes in a Good Solvent Mixture. *Soft Matter* **2019**, *15* (39), 7968–7980, DOI 10.1039/c9sm01123d.
- (18) Yong, H.; Bittrich, E.; Uhlmann, P.; Fery, A.; Sommer, J. U. Co-Nonsolvency Transition of Poly(N-Isopropylacrylamide) Brushes in a Series of Binary Mixtures. *Macromolecules* **2019**, *52* (16), 6285–6293, DOI 10.1021/acs.macromol.9b01286.
- (19) Yong, H.; Molcrette, B.; Sperling, M.; Montel, F.; Sommer, J. U. Regulating the Translocation of DNA through Poly(N-Isopropylacrylamide)-Decorated Switchable Nanopores by Cononsolvency Effect. *Macromolecules* **2021**, *54* (9), 4432–4442, DOI 10.1021/acs.macromol.1c00215.
- (20) Yu, Y.; Lopez De La Cruz, R. A.; Kieviet, B. D.; Gojzewski, H.; Pons, A.; Julius Vancso, G.; De Beer, S. Pick up, Move and Release of Nanoparticles Utilizing Co-Non-Solvency of PNIPAM Brushes. *Nanoscale* **2017**, *9* (4), 1670–1675, DOI 10.1039/c6nr09245d.
- (21) Kong, C.; Kanezashi, M.; Yamomoto, T.; Shintani, T.; Tsuru, T. Controlled Synthesis of High Performance Polyamide Membrane with Thin Dense Layer for Water Desalination. *J. Memb. Sci.* **2010**, *362* (1–2), 76–80, DOI 10.1016/j.memsci.2010.06.022.
- (22) Kong, C.; Shintani, T.; Kamada, T.; Freger, V.; Tsuru, T. Co-Solvent-Mediated Synthesis of Thin Polyamide Membranes. *J. Memb. Sci.* **2011**, *384* (1–2), 10–16, DOI 10.1016/j.memsci.2011.08.055.
- (23) Li, C. W.; Merlitz, H.; Wu, C. X.; Sommer, J. U. Nanopores as Switchable Gates for Nanoparticles: A Molecular Dynamics Study. *Macromolecules* **2018**, *51* (16), 6238–6247, DOI 10.1021/acs.macromol.8b01149.
- (24) Birshtein, T. M.; Lyatskaya, Y. V. Polymer Brush in a Mixed Solvent. *Colloids Surfaces A Physicochem. Eng. Asp.* **1994**, *86* (C), 77–83, DOI 10.1016/0927-7757(94)02841-9.
- (25) Lai, P. Y.; Halperin, A. Polymer Brushes in Mixed Solvents: Chromatography and Collapse. *Macromolecules* **1992**, *25* (24), 6693–6695, DOI 10.1021/ma00050a045.
- (26) Li, C.; Zhang, T.; Yang, Y.; Tang, P.; Qiu, F. Polymer Brushes Immersed in Two-Component Solvents with Pure Volume Exclusion: Effect of Solvent Molecular Shape. *ACS Omega* **2019**, *4* (7), 12927–12937, DOI 10.1021/acsomega.9b01800.
- (27) Lim, R. Y. H.; Deng, J. Interaction Forces and Reversible Collapse of a Polymer Brush-

- Gated Nanopore. ACS Nano 2009, 3 (10), 2911–2918, DOI 10.1021/nn900152m.
- (28) Coalson, R. D.; Eskandari Nasrabad, A.; Jasnow, D.; Zilman, A. A Polymer-Brush-Based Nanovalve Controlled by Nanoparticle Additives: Design Principles. *J. Phys. Chem. B* **2015**, *119* (35), 11858–11866, DOI 10.1021/acs.jpcb.5b02623.
- (29) Ma, T.; Arroyo, N.; Janot, J. M.; Picaud, F.; Balme, S. Conformation of Polyethylene Glycol inside Confined Space: Simulation and Experimental Approaches. *Nanomaterials* **2021**, *11* (1), 1–18, DOI 10.3390/nano11010244.
- (30) Emilsson, G.; Xiong, K.; Sakiyama, Y.; Malekian, B.; Ahlberg Gagnér, V.; Schoch, R. L.; Lim, R. Y. H.; Dahlin, A. B. Polymer Brushes in Solid-State Nanopores Form an Impenetrable Entropic Barrier for Proteins. *Nanoscale* **2018**, *10* (10), 4663–4669, DOI 10.1039/c7nr09432a.
- (31) Lee, J. H.; Lee, H. B.; Andrade, J. D. Blood Compatibility of Polyethylene Oxide Surfaces. *Prog. Polym. Sci.* **1995**, *20* (6), 1043–1079, DOI 10.1016/0079-6700(95)00011-4.
- (32) Awasthi, S.; Sriboonpeng, P.; Ying, C.; Houghtaling, J.; Shorubalko, I.; Marion, S.; Davis, S. J.; Sola, L.; Chiari, M.; Radenovic, A.; Mayer, M. Polymer Coatings to Minimize Protein Adsorption in Solid-State Nanopores. *Small Methods* **2020**, *4* (11), 1–10, DOI 10.1002/smtd.202000177.
- (33) Gon, S.; Kumar, K. N.; Nüsslein, K.; Santore, M. M. How Bacteria Adhere to Brushy PEG Surfaces: Clinging to Flaws and Compressing the Brush. *Macromolecules* **2012**, *45* (20), 8373–8381, DOI 10.1021/ma300981r.
- (34) Chen, G.; Dormidontova, E. PEO-Grafted Gold Nanopore: Grafting Density, Chain Length, and Curvature Effects. *Macromolecules* **2022**, *55* (12), 5222–5232, DOI 10.1021/acs.macromol.2c00323.
- (35) Dahal, U. R.; Dormidontova, E. E. The Dynamics of Solvation Dictates the Conformation of Polyethylene Oxide in Aqueous, Isobutyric Acid and Binary Solutions. *Phys. Chem. Chem. Phys.* **2017**, *19* (15), 9823–9832, DOI 10.1039/c7cp00526a.
- (36) Dahanayake, R.; Dahal, U.; Dormidontova, E. E. Co-Solvent and Temperature Effect on Conformation and Hydration of Polypropylene and Polyethylene Oxides in Aqueous Solutions. *J. Mol. Liq.* **2022**, *362*, 119774, DOI 10.1016/j.molliq.2022.119774.
- (37) Van Der Spoel, D.; Lindahl, E.; Hess, B.; Groenhof, G.; Mark, A. E.; Berendsen, H. J. C. GROMACS: Fast, Flexible, and Free. *J. Comput. Chem.* **2005**, *26* (16), 1701–1718, DOI 10.1002/jcc.20291.
- (38) Towns, J.; Cockerill, T.; Dahan, M.; Foster, I.; Gaither, K.; Grimshaw, A.; Hazlewood, V.; Lathrop, S.; Lifka, D.; Peterson, G. D.; Roskies, R.; Scott, J. ray; Wilkins-Diehr, N. Accelerating Scientific Discovery. *Comput. Sci. Eng.* **2014**, *16* (5), 62–74.
- (39) Tay, K. A.; Bresme, F. Wetting Properties of Passivated Metal Nanocrystals at Liquid-Vapor Interfaces: A Computer Simulation Study. *J. Am. Chem. Soc.* **2006**, *128* (43),

- 14166-14175, DOI 10.1021/ja061901w.
- (40) Chen, G. PolyGraft 1.0: A Program for Molecular Structure and Topology Generation of Polymer-grafted Hybrid Nanostructures. *J. Comput. Chem.* **2023**, *44* (28), 2230–2239, DOI 10.1002/jcc.27206.
- (41) Berendsen, H. J. C.; Grigera, J. R.; Straatsma, T. P. The Missing Term in Effective Pair Potentials. *J. Phys. Chem.* **1987**, *91* (24), 6269–6271, DOI 10.1021/j100308a038.
- (42) Jorgensen, W. L.; Maxwell, D. S.; Tirado-Rives, J. Development and Testing of the OPLS All-Atom Force Field on Conformational Energetics and Properties of Organic Liquids. *J. Am. Chem. Soc.* **1996**, *118* (45), 11225–11236, DOI 10.1021/ja9621760.
- (43) Zangi, R. Refinement of the OPLSAA Force-Field for Liquid Alcohols. *ACS Omega* **2018**, 3 (12), 18089–18099, DOI 10.1021/acsomega.8b03132.
- (44) Barden, W. R. T.; Singh, S.; Kruse, P. Roughening of Gold Atomic Steps Induced by Interaction with Tetrahydrofuran. *Langmuir* **2008**, *24* (6), 2452–2458, DOI 10.1021/la701757e.
- (45) Mountain, R. D.; Wallqvist, A. A Collection of Results for SPC/E Water Model. **1996**, No. NISTIR 5778.